

Fractional quantum-Hall liquid spontaneously generated by strongly correlated t_{2g} electrons

Jörn Venderbos, Stefanos Kourtis, Jeroen van den Brink, and Maria Daghofer
Institute for Theoretical Solid State Physics, IFW Dresden, 01171 Dresden, Germany
 (Dated: September 22, 2022)

For topologically nontrivial and very narrow bands, Coulomb repulsion between electrons has been predicted to give rise to a spontaneous fractional quantum-Hall (FQH) state in absence of magnetic fields. Here we show that strongly correlated electrons in a t_{2g} -orbital system on a triangular lattice self-organize into a spin-chiral magnetic ordering pattern that induces precisely the required topologically nontrivial and flat bands. We show that this behavior is very robust and does not rely on fine tuning. On top of a self-consistent mean-field approach, we use exact diagonalization to study an effective one-band model for the emerging flat band in the presence of longer-range interactions and establish the signatures of a spontaneous $\nu = 1/3$ FQH state.

The Integer Quantum Hall (IQH) effect [1] is a prime example of an electronic state that cannot be classified within the traditional framework of symmetry breaking, but is instead characterized by a topological invariant [2]. It is by now theoretically well established that an external magnetic field is in principle not needed and that states within the same topological class as IQH states can be realized in lattice models, if time-reversal symmetry is broken by other mechanisms, e.g., by complex electron hoppings [3]. Related topologically nontrivial Quantum Spin-Hall (QSH) states even occur in systems where time-reversal symmetry is not broken at all [4–7], see Refs. [8, 9] for reviews. At present, many intriguing features intrinsic to topologically non-trivial states have been observed in the absence of magnetic fields, such as the metallic Dirac cones at the surface of a topological insulator [10, 11], or the QSH effect in quantum wells [12, 13].

Fractional Quantum Hall (FQH) states [14] are topological states that can be seen as composed of quasi-particles carrying an exact fraction of the elementary electronic charge [15]. Apart from the fundamental interest in observing a quasi-particle that behaves in many ways like a fraction of an electron, some FQH states also have properties relevant to fault-tolerant quantum computation [16]. Very recently [17–19], it was suggested that lattice-FQH states [20] may similarly arise without a magnetic field, in fractionally filled topologically non-trivial bands.

In contrast to the IQH and QSH effects, which can be fully understood in terms of non-(or weakly-)interacting electrons, interactions are an essential requirement for FQH states, which places demanding restrictions on candidate systems: One needs a topologically nontrivial band that must be nearly flat – similar to the highly degenerate Landau levels – so that the electron-electron interaction can at the same time be large compared to the band width and small compared to the gap separating it from other bands [17–19]. If the requirements can be fulfilled, however, the temperature scale of the FQH state is set by the energy scale of the interaction.

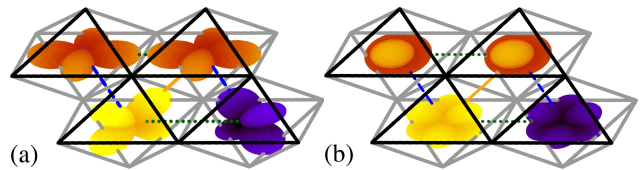


FIG. 1. (Color online) Triangular perovskite lattice and t_{2g} orbitals. Oxygen octahedra are indicated by lines, with black lines illustrating the front facets. Thick dotted (dashed, solid) lines indicate nearest-neighbor bonds along lattice vector \mathbf{a}_1 (\mathbf{a}_2 , \mathbf{a}_3). (a) Shows two d_{xy} orbitals (top) and one d_{xz} and d_{yz} orbital (bottom). In (b), the orbitals reflecting the three-fold lattice symmetry are shown: The two e'_g orbitals (bottom), which differ by their complex phases, will turn out to be half filled, while the a_{1g} orbital (pointing out of the plane, see top) forms nearly flat bands with non-trivial topological character that can support spontaneous FQH states.

This can allow temperatures considerably higher than the sub-Kelvin range of the conventional FQH effect, which would be extremely desirable in view of potential quantum-computing applications.

In all recently proposed model Hamiltonians [17–19, 21–23], the topological nature of the bands was introduced by hand and model parameters were carefully tuned to obtain very flat bands. On the other hand, topologically nontrivial bands can in principle emerge spontaneously in interacting electron systems [24], e.g., for charge-ordered systems [25, 26] or for electrons coupling to spins in a non-coplanar magnetic order [27, 28]. We demonstrate here that such a scenario indeed arises in a Hubbard model describing electrons with a t_{2g} orbital degree of freedom on a triangular lattice: a ground state with topologically nontrivial and nearly flat bands is stabilized by onsite Coulomb interactions, and upon doping the flat bands, longer-range Coulomb repulsion induces a FQH state.

t_{2g} orbitals on the triangular lattice.— The building blocks of our system are oxygen octahedra with a transition-metal (TM) ion in the center, the most common building block in the large and versatile material

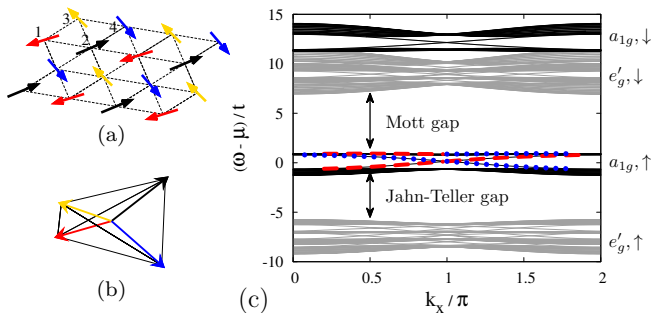


FIG. 2. (Color online) Spin-chiral magnetic phase with topologically nontrivial bands stabilized by onsite Coulomb interactions in t_{2g} electrons on a triangular lattice. (a) Chiral magnetic order, the sites of the unit cell are labeled by 1 to 4. (b) The spins on the four sites can be seen as pointing to the corners of a tetrahedron, i.e., the pattern is non-coplanar. (c) One-particle energies on a cylinder (periodic boundary conditions along x) in the mean-field [31] ground state of the t_{2g} multiorbital Hubbard model, which is given by the pattern shown in (a). States drawn in black (grey) have more (less) than 33% a_{1g} character, dashed and dotted lines indicates edge states with more than 33% of their weight on the top (bottom) row of sites. The arrows \uparrow (\downarrow) indicate states with electron spin mostly (anti-)parallel to the local quantization axis, which can be seen as the lower (upper) Hubbard band. The filling is 2.5 electrons per site, slightly less than half filling. Parameters used were $t = 1$, $t_{dd} = 0$, $U/t = 12$, $J/t = 3$, $\Delta_{JT}/t = -6$. The figure of merit M , which is given by the ratio of the gap separating the two a_{1g} subbands of the lower Hubbard band and the band width of the highest subband of the lower Hubbard band, is $M \approx 14$.

class of TM oxides. Local cubic symmetry due to the oxygen ions splits the d -orbitals into t_{2g} and e_g levels, and it has been shown that orbital degrees of freedom of either kind can substantially reduce the width of topologically nontrivial bands [22]. Here, we concentrate on the t_{2g} orbitals illustrated in Fig. 1(a), which are further split by a crystal-field due to the overall lattice geometry. On a triangular lattice, we find one a_{1g} and two $e'_{g,\pm}$ states, see Fig. 1(b), with a splitting $H_{JT} = \Delta_{JT}(n_{e_{g+}} + n_{e_{g-}} - 2n_{a_{1g}})/3$ depending on the Jahn-Teller effect and the lattice [29]. Electron hopping along nearest-neighbor (NN) bonds consists of terms t via ligand oxygens and t_{dd} due to direct d - d overlap [29, 30], hopping matrices are given in [31]. We set here $n < 3$ and choose $t > 0$ [29] as unit of energy, but analogous results hold for $n > 3$, $t < 0$, and $t_{dd} \rightarrow -t_{dd}$, $\Delta_{JT} \rightarrow -\Delta_{JT}$ due to particle-hole symmetry.

In TM oxides, Coulomb interaction is substantial compared to the kinetic energy of t_{2g} orbitals and spin-orbital physics induced by correlations are known to be rich in t_{2g} systems on triangular lattices [30, 32]. We take into account the onsite interaction including Coulomb repulsion U (intra-orbital) and U' (interorbital) as well as Hund's-rule coupling J . We employ a mean-field approximation with a decoupling into expectation values

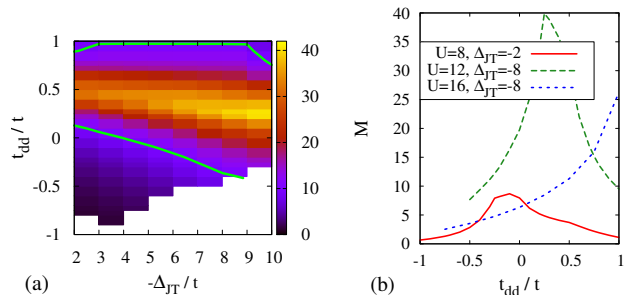


FIG. 3. (Color online) Stability of the spin-chiral phase and flatness of the topological bands depending on parameters of the Hamiltonian. In (a), shaded areas in the t_{dd} - Δ_{JT} plane indicate a spin-chiral ground state Fig. 2(a,b) for $U/t = 12$, white areas have a different ground state. Shading indicates the figure of merit M for the flatness of the upper chiral subband, bright thick lines bound the region with $M \geq 10$. (b) shows M depending on t_{dd} for selected sets of U and Δ_{JT} . Where the ‘‘Mott gap’’, which separates the flat topologically non-trivial band from the upper Hubbard band, becomes very small, M is determined by the minimal gap separating the band of interest from other bands. $J = U/4$ and $t = 1$ were used in all cases.

of densities $\langle n_{\mathbf{i},\alpha,\sigma} \rangle = \langle c_{\mathbf{i},\alpha,\sigma}^\dagger c_{\mathbf{i},\alpha,\sigma} \rangle$ for site \mathbf{i} , orbital α , and spin σ [33, 34]. The spin is thus reduced to its z -component $m_{\mathbf{i},\alpha} = (n_{\mathbf{i},\alpha,\uparrow} - n_{\mathbf{i},\alpha,\downarrow})/2$ and non-collinear magnetic patterns are treated by allowing for a site-dependent spin-quantization axis expressed by angles θ_i and ϕ_i . The change in quantization axis from site to site manifests itself in a complex Berry phase for the hopping terms [35]. Numerical optimization is used to find the θ_i and ϕ_i giving the magnetic ground state, permitting arbitrary magnetic orderings with unit cells of up to four sites, including all phases considered in Ref. [36]. For simplicity, we present here results for $J/U = 1/4$ and the relation $U' = U - 2J$ between the Kanamori parameters was used, but we have verified that the results presented remain robust for other choices. For details see [31].

For wide parameter ranges (see below), the ground state is the non-coplanar spin-chiral phase illustrated in Fig. 2(a,b). As demonstrated in the context of the Kondo-lattice model [34, 36], this magnetic order leads to topologically nontrivial bands, which can also be seen in the one-particle bands shown in Fig. 2(c). The chemical potential lies within the a_{1g} states of the lower Hubbard band, where the electron spin is mostly parallel (labelled by \uparrow) to the direction defined by the spin-chiral pattern. Dashed and dotted lines decorate states living on the top and bottom edges of a cylinder, they cross the chiral gap exactly once as one left- and one right-moving edge mode, indicating the different Chern numbers associated with the two bands directly above and below the chemical potential.

Figure 2(c) also indicates that the upper chiral subband has a very small width, ~ 14 times smaller than

the chiral gap. One can quantify the band flatness by a figure of merit M given by the ratio of the gap to the band width. Its dependence on various parameters of the Hamiltonian is shown in Fig. 3. It peaks at $M > 40$, but the more striking observation is that it is above 5 or even 10 for wide ranges of U , Δ_{JT} and t_{dd} , in contrast to many other proposals that require carefully fine-tuned parameters [17–19, 21–23, 37]. Nearly flat chiral bands are thus very robust in this system and both their topological character and their flat dispersion emerge spontaneously with purely onsite interaction and short-range hopping, without spin-orbit coupling or any explicit breaking of time-reversal symmetry.

In order to understand the origin of the spin-chiral state, it is helpful to look at the one-band Kondo-lattice model (KLM), which describes itinerant electrons coupled to localized spins. The KLM supports spin-chiral phases because of frustration between ferromagnetism (driven by double exchange, i.e., the kinetic energy of the electrons) and antiferromagnetism (driven by superexchange between the localized spins) on many frustrated lattices like the triangular [34, 36, 38, 39], pyrochlore [40], and face-centered cubic [41] lattices. Our model can be related to the KLM by noting that the half-filled e'_g levels are far from the chemical potential and act as a localized spin to which the electrons in the a_{1g} orbital are coupled via Hund's rule coupling. The antiferromagnetic superexchange arises through excitations into the upper Hubbard band. Consequently, it is suppressed by a larger Mott gap and the ground state becomes ferromagnetic for $U \gtrsim 24|t|$, as in the KLM with a large Kondo gap [36, 38]. In a large window $6 \lesssim U/|t| \lesssim 24$, the balance of kinetic energy and superexchange stabilizes a spin-chiral ground state and flat bands with $M > 5$ are found for a window of $8 \lesssim U/|t| \lesssim 20$.

FQH groundstate of an effective spinless one-band model.— The nearly flat band of interest is mostly given by the a_{1g} orbital, whose hopping is isotropic in the absence of magnetic order. The flat band lies in the lower Hubbard/Kondo band and the electron spin is predominantly parallel to the spin-chiral background formed by the more localized e'_g levels. We can thus map the a_{1g} system onto spinless fermions, where the impact of the spin-chiral order is reflected in complex hoppings due to Berry phases. Virtual excitations into the e'_g states and the upper Hubbard/Kondo band additionally induce effective longer-range hopping. In the simpler case of an infinite Kondo gap, where the band flattening also occurs [22], second-neighbor hopping drops out due to destructive interference between two equivalent hopping paths and the effective Hamiltonian is

$$H_{\text{eff}}(\mathbf{k}) = 2t_1 \sum_j \sigma^j \cos \mathbf{k}\mathbf{a}_j + 2t_3 \sum_j \sigma^0 \cos 2\mathbf{k}\mathbf{a}_j, \quad (1)$$

where \mathbf{a}_j ($j = 1, 2, 3$) denote the unit vectors on the triangular lattice. Pauli matrices σ^j and unit matrix

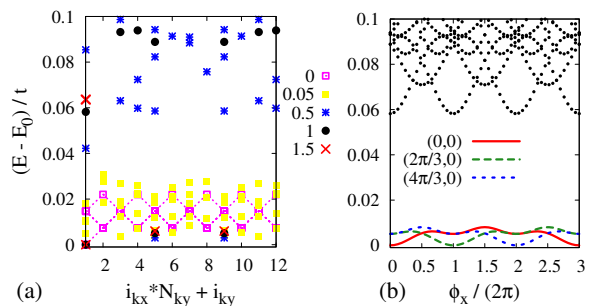


FIG. 4. (Color online) FQH state induced by NN Coulomb repulsion V in the effective one-band model Eq. 1. (a) Energy depending on total momentum \mathbf{k} for several values of V/t . (Only the five lowest energies are plotted for each \mathbf{k} , i.e., the spectrum for the small $V = 0, 0.05$ does extend to higher energies.) (b) Energy for $V/t = 1$ depending on a flux ϕ_x added whenever an electron goes once around the whole lattice in x direction. Each addition of $\phi = 2\pi$ leads to an equivalent state, 6π to the same state. The Chern numbers associated with the three low-energy states for $V/t = 1$ are 0.32, 0.34 and 0.34. Lattice size is 6×4 sites (12 two-site unit cells), parameters of the effective one-band model are $t_1 = 0.27|t|$ and $t_3 = 0.06|t|$, which describes chiral bands with $M \approx 13$ and a chiral gap of $0.89|t|$. The filling was set to give $1/3$ filling of the flat band.

σ^0 refer to the two sites of the electronic unit cell in the chiral phase [34], this unit cell and the topologically nontrivial bands arise through the symmetry breaking involved in the magnetic order. Perturbation theory gives in this case effective third-neighbor hopping $t_3 = -2(t - t_{dd})^2 / (27\Delta_{\text{JT}})$ in addition to NN hopping $t_1 = (2t + t_{dd}) / 3\sqrt{3}$; we set here $t = 1$, $t_{dd}/t = -0.6$, and $\Delta_{\text{JT}}/t = -10/3$, which leads to $t_1 = 0.27|t|$ and $t_3 = 0.06|t|$ and provides a good fit to chiral bands with a figure of merit $M \approx 13$ and a chiral gap of $0.89|t|$. This is similar to the case illustrated in Fig. 2(c), but with the flat subband below the gap; a filling fraction of $1/n$ in the desired band thus implies a total electron density of $1/(2n)$. Formally, the effective model (1) describes electrons moving in a constant (and very strong) magnetic field with a flux of $\pi/2$ threading each triangle of the lattice [34].

We now check whether longer-range (i.e., beyond onsite) Coulomb interactions stabilize a FQH ground state in the fractionally filled narrow band; the effective one-orbital model Eq. (1) allows us to treat the full interacting many-body problem including NN Coulomb interaction $V \sum_{\langle i,j \rangle} n_i n_j$ on small clusters with Lanczos exact diagonalization [19, 37, 42], see also [31]. It should be noted that the nearest-neighbor bonds $\langle i,j \rangle$ are defined on the original triangular lattice, i.e., V acts both between the two sites within one unit cell and between NN sites belonging to different unit cells. We consider here for illustration the simplest case with $1/3$ filling,

i.e. a total electron density of $1/6$. Figure 4 indicates that V induces signatures of a $\nu = 1/3$ FQH ground state for 12 electrons on a 6×4 lattice: three nearly degenerate states become separated from higher-energy states by a gap. Inserting a magnetic flux $\phi_x = 2\pi$ interchanges the three states, $\phi_x = 6\pi$ recovers the original situation, as reported for other systems [19, 22, 37]. The Chern number C can be evaluated by integrating the flux-dependent Berry curvature $\Omega^n(\phi_x, \phi_y)$ over the square $0 \leq \phi_x, \phi_y < 2\pi$, and $\Omega^n(\phi_x, \phi_y)$ is obtained by the Kubo formula [31, 43, 44]. For the three low-energy states and $V = |t|$, we find $C = 0.32, 0.34$, and 0.34 , adding to 1. These values come very close to the expected $C = 1/3$ and the small deviation is well within the limits of reported finite-size effects [19].

Conclusions.— The possibility of a spontaneous FQH effect without a magnetic field is currently hotly discussed, and various models have been suggested [17–19, 21–23, 37]. In these proposals, the necessary topological character of the bands was introduced by hand, the flatness of the bands needed fine-tuning and the underlying lattices were often rather exotic; an experimental realization appears therefore challenging. We have shown here that in strongly correlated t_{2g} orbitals on a triangular lattice, bands with the desired properties emerge spontaneously for wide parameter ranges and support FQH ground states. Both t_{2g} systems and triangular lattices occur in various TM oxides, and signatures of the unconventional *integer* QH state have been reported for a triangular-lattice palladium-chromium oxide [45]. This harbors the prospect that a suitable material can be synthesized in this highly versatile material class. As such a material is by default strongly correlated, one also naturally expects an inter-site Coulomb repulsion that is strong enough to stabilize spontaneous FQH states in the absence of a magnetic field.

This research was supported by DFG (Emmy-Noether program; SK and MD) and the Interphase Program of the Dutch Science Foundation NWO/FOM (JV and JvdB).

The appendix contains Supplemental Material:

One-particle terms of the multi-orbital t_{2g} Hamiltonian

The multi-orbital kinetic energy is

$$H_{\text{kin}} = \sum_{\langle i,j \rangle, \alpha, \beta, \sigma} t_{i,j}^{\alpha, \beta} c_{i,\alpha,\sigma}^\dagger c_{j,\beta,\sigma} + \text{H.c.}, \quad (2)$$

where $c_{i,\alpha,\sigma}^\dagger$ ($c_{i,\alpha,\sigma}$) creates (annihilates) an electron on site i , in orbital α and with spin σ . $\langle i, j \rangle$ denotes nearest-neighbor (NN) bonds, α and β denote the orbital. Using as basis states the xy , xz , and yz orbitals shown in

Fig. 1(a) of the main text, the orbital- and direction-dependent hopping parameters $t_{i,j}^{\alpha, \beta}$ are given by the matrices

$$\hat{T}_1 = \begin{pmatrix} t_{dd} & 0 & 0 \\ 0 & 0 & t \\ 0 & t & 0 \end{pmatrix}, \quad \hat{T}_2 = \begin{pmatrix} 0 & 0 & t \\ 0 & t_{dd} & 0 \\ t & 0 & 0 \end{pmatrix}, \quad \hat{T}_3 = \begin{pmatrix} 0 & t & 0 \\ t & 0 & 0 \\ 0 & 0 & t_{dd} \end{pmatrix}$$

for NN bonds along the three directions $\mathbf{a}_1, \mathbf{a}_2, \mathbf{a}_3$ as illustrated in Fig. 1 of the main text. The transformation into the $\{a_{1g}, e'_{g,+}, e'_{g,-}\}$ can be found, e.g., in Ref. [29].

Mean-field approximation

Onsite interaction is described by Kanamori parameters U (U') for Coulomb repulsion between electrons in the same (different) orbitals as well as ferromagnetic Hund's-rule coupling between electrons in different orbitals. The relation $U' = U - 2J$ is used here, ‘‘pair-hopping’’ J' is left out, because it drops out of the mean field decoupling

$$\begin{aligned} H_{\text{int}} \approx & U \sum_{\mathbf{i}, \alpha} (\langle n_{\mathbf{i}, \alpha, \uparrow} \rangle n_{\mathbf{i}, \alpha, \downarrow} + n_{\mathbf{i}, \alpha, \uparrow} \langle n_{\mathbf{i}, \alpha, \downarrow} \rangle) \\ & + (U' - J/2) \sum_{\mathbf{i}, \alpha < \beta} (\langle n_{\mathbf{i}, \alpha} \rangle n_{\mathbf{i}, \beta} + n_{\mathbf{i}, \alpha} \langle n_{\mathbf{i}, \beta} \rangle) \\ & - 2J \sum_{\mathbf{i}, \alpha < \beta} (\langle m_{\mathbf{i}, \alpha} \rangle m_{\mathbf{i}, \beta} + m_{\mathbf{i}, \alpha} \langle m_{\mathbf{i}, \beta} \rangle) \\ & - U \sum_{\mathbf{i}, \alpha} \langle n_{\mathbf{i}, \alpha, \uparrow} \rangle \langle n_{\mathbf{i}, \alpha, \downarrow} \rangle - (U' - J/2) \sum_{\mathbf{i}, \alpha < \beta} \langle n_{\mathbf{i}, \alpha} \rangle \langle n_{\mathbf{i}, \beta} \rangle \\ & + 2J \sum_{\mathbf{i}, \alpha < \beta} \langle m_{\mathbf{i}, \alpha} \rangle \langle m_{\mathbf{i}, \beta} \rangle, \end{aligned} \quad (3)$$

where \mathbf{i} labels the site, α and β orbitals. $n_{\mathbf{i}, \alpha, \sigma} = c_{\mathbf{i}, \alpha, \sigma}^\dagger c_{\mathbf{i}, \alpha, \sigma}$ is the density operator. We keep here only expectation values for diagonal operators, i.e., only $\langle n_{\mathbf{i}, \alpha, \sigma} \rangle = \langle c_{\mathbf{i}, \alpha, \sigma}^\dagger c_{\mathbf{i}, \alpha, \sigma} \rangle$ [33, 34], which reduces the spin to its z -component $m_{\mathbf{i}, \alpha} = (n_{\mathbf{i}, \alpha, \uparrow} - n_{\mathbf{i}, \alpha, \downarrow})/2$. In order to treat non-collinear spin patterns, one has to allow for a site-dependent spin-quantization axis given by angles θ_i and ϕ_i . The change in quantization axis from site to site manifests itself in a complex phase for the hopping terms, [35] which is between sites i and j

$$\begin{aligned} \Omega_{ij}^{\sigma, \sigma} &= \cos \frac{\theta_i}{2} \cos \frac{\theta_j}{2} + \sin \frac{\theta_i}{2} \sin \frac{\theta_j}{2} e^{-i\sigma(\phi_i - \phi_j)} \\ \Omega_{ij}^{\uparrow, \downarrow} &= \cos \frac{\theta_i}{2} \sin \frac{\theta_j}{2} e^{-i\phi_j} - \cos \frac{\theta_j}{2} \sin \frac{\theta_i}{2} e^{-i\phi_i} \end{aligned} \quad (4)$$

where $\Omega_{ij}^{\uparrow, \uparrow}$ ($\Omega_{ij}^{\downarrow, \downarrow}$) modulates the hopping of an electron with spin parallel (antiparallel) to the chosen spin-quantization axis. In the site-dependent quantization, spin is not conserved and there are spin-mixing hoppings with $\Omega_{ij}^{\downarrow, \uparrow}$ given by the complex conjugate of $\Omega_{ji}^{\uparrow, \downarrow}$.

We use numerical optimization routines to find the spin pattern with the lowest energy among all orderings with unit cells of up to four sites, including all patterns considered in Ref. [36] of the main text. In each step, the mean-field energy is calculated self-consistently for a lattice of 16×16 (four-site unit cell) or 24×16 (three-site unit cell). (For selected points in parameter space, we also used larger lattices and did not find a significant difference.) In order to minimize the impact of our approximations on the symmetries of the orbital degrees of freedom, we perform the mean-field decoupling in the $\{a_{1g}, e'_{g,+}, e'_{g,-}\}$ basis, where the symmetry between the half-filled $e'_{g,+}$ and the quarter-filled a_{1g} orbitals (for the fillings discussed here) is already broken by the crystal field. We verified that decoupling directly in the $\{xy, xz, yz\}$ basis, where all three orbitals have the same electronic density, leads to qualitatively identical and quantitatively very similar results.

Effective one-band model and exact diagonalization

The mapping to the effective one-band model is most easily carried out in the Kondo-lattice picture, where the localized spins are assumed to consist of the e'_g electrons. Without a magnetic order, the a_{1g} orbital has an isotropic hopping $(2t + t_{dd})/3$, i.e., the same along all three directions on the triangular lattice, but in the spin-chiral phase, this hopping is modulated by a direction-dependent Berry phase Eq. (4). The electronic unit cell of the spin-chiral pattern has two sites [34], and the Berry phases can then be expressed in terms of Pauli matrices as given in the main text. The absolute value of the NN hopping is renormalized to $t_1 = (2t + t_{dd})/3\sqrt{3}$. Corrections to this simplest approximation can be obtained by second-order perturbation theory, which yields longer-range hopping processes mediated by virtual excitations of holes into e'_g levels or electrons into the upper Hubbard/Kondo band. The band flattening also occurs in the limit of an infinite Kondo gap [22], and in

this simpler case, second-neighbour hopping drops out due to destructive interference between two equivalent hopping paths. In this limit of a large Hubbard/Kondo gap, perturbation theory leads third-neighbour hopping $t_3 = -2(t - t_{dd})^2/(27\Delta_{JT})$.

In order to investigate the FQH groundstate, we used Lanczos exact diagonalization to study the Hamiltonian given by the kinetic energy of the effective one-band model, Eq. (1) of the main text, and NN Coulomb repulsion $V \sum_{\langle i,j \rangle} n_i n_j$. As pointed out in the main text, nearest-neighbour bonds $\langle i, j \rangle$ are defined on the original triangular lattice and V acts both between the two sites within one unit cell and between NN sites belonging to different unit cells. We studied systems with 6×4 and 6×6 sites, i.e., with 12 and 18 two-site unit cells, with 4 and 6 electrons, resp. In both systems, we find three nearly degenerate ground states separated from higher-energy states by a gap.

Inserting a flux (ϕ_x, ϕ_y) means that electrons gain a phase $e^{i\phi_x}$ ($e^{i\phi_y}$) for going once around the whole lattice in x -(y -) direction. This is implemented by changing the hopping $t_{i,j}$ from site $\mathbf{i} = i_x \mathbf{a}_1 + i_y \mathbf{a}_2$ to site $\mathbf{j} = j_x \mathbf{a}_1 + j_y \mathbf{a}_2$ to

$$t_{i,j} \rightarrow t_{i,j} e^{i\left(\phi_x \frac{j_x - i_x}{L_x} + \phi_y \frac{j_y - i_y}{L_y}\right)}, \quad (5)$$

leading to a flux-dependent Hamiltonian $H_{\text{eff}}(\phi_x, \phi_y)$. In the 6×6 system, we likewise find three low-energy states separated from the remaining spectrum by a gap, but all three low-energy states have total momentum $(0, 0)$ for $(\phi_x, \phi_y) = (0, 0)$. Due to finite-size effects, the states do then not cross upon flux insertion [42], but avoid crossings. For the smaller 6×4 system, the three low-energy states have different total momenta, and this good quantum number allows us to clearly resolve their crossing when we insert a flux ϕ_x , even on a finite system.

The Chern numbers were evaluated by integrating the Berry curvature $\Omega^n(\phi_x, \phi_y)$ over the square $0 \leq \phi_x, \phi_y < 2\pi$. $\Omega^n(\phi_x, \phi_y)$ was obtained by the Kubo formula [43, 44]

$$\Omega^n(\phi_x, \phi_y) = iL_x L_y \sum_{n' \neq n} \frac{\langle n | \frac{\partial H_{\text{eff}}(\phi_x, \phi_y)}{\partial \phi_x} | n' \rangle \langle n' | \frac{\partial H_{\text{eff}}(\phi_x, \phi_y)}{\partial \phi_y} | n \rangle - \langle n | \frac{\partial H_{\text{eff}}(\phi_x, \phi_y)}{\partial \phi_y} | n' \rangle \langle n' | \frac{\partial H_{\text{eff}}(\phi_x, \phi_y)}{\partial \phi_x} | n \rangle}{(\epsilon_n - \epsilon_{n'})^2}, \quad (6)$$

where n' and n label eigenstates with energies $\epsilon_{n'}/n$ and $\partial H_{\text{eff}}(\phi_x, \phi_y)/\partial \phi_{x/y}$ are current operators.

[1] K. v. Klitzing, G. Dorda, and M. Pepper, Phys. Rev. Lett. **45**, 494 (1980).

[2] D. J. Thouless, M. Kohmoto, M. P. Nightingale, and M. den Nijs, Phys. Rev. Lett. **49**, 405 (1982).

[3] F. D. M. Haldane, Phys. Rev. Lett. **61**, 2015 (1988).

[4] C. L. Kane and E. J. Mele, Phys. Rev. Lett. **95**, 146802 (2005).

[5] L. Fu, C. L. Kane, and E. J. Mele, Phys. Rev. Lett. **98**, 106803 (2007).

[6] R. Roy, Phys. Rev. B **79**, 195322 (2009).

- [7] J. E. Moore and L. Balents, Phys. Rev. B **75**, 121306 (2007).
- [8] M. Hasan and C. Kane, Rev. Mod. Phys. **82**, 3045 (2010).
- [9] X.-L. Qi and S.-C. Zhang, arXiv:1008.2026.
- [10] H. Zhang, C.-X. Liu, X.-L. Qi, X. Dai, Z. Fang, and S.-C. Zhang, Nature Phys. **5**, 438 (2009).
- [11] Y. Xia, D. Qian, D. Hsieh, L. Wray, A. Pal, H. Lin, A. Bansil, D. Grauer, Y. S. Hor, R. J. Cava, and M. Z. Hasan, Nature Phys. **5**, 398 (2009).
- [12] B. A. Bernevig, T. L. Hughes, and S.-C. Zhang, Science **314**, 1757 (2006).
- [13] M. König, S. Wiedmann, C. Brüne, A. Roth, H. Buhmann, L. W. Molenkamp, X.-L. Qi, and S.-C. Zhang, Science **318**, 766 (2007).
- [14] D. C. Tsui, H. L. Stormer, and A. C. Gossard, Phys. Rev. Lett. **48**, 1559 (1982).
- [15] R. B. Laughlin, Phys. Rev. Lett. **50**, 1395 (1983).
- [16] C. Nayak, S. H. Simon, A. Stern, M. Freedman, and S. Das Sarma, Rev. Mod. Phys. **80**, 1083 (2008).
- [17] E. Tang, J.-W. Mei, and X.-G. Wen, Phys. Rev. Lett. **106**, 236802 (2011).
- [18] K. Sun, Z. Gu, H. Katsura, and S. D. Sarma, Phys. Rev. Lett. **106**, 236803 (2011).
- [19] T. Neupert, L. Santos, C. Chamon, and C. Mudry, Phys. Rev. Lett. **106**, 236804 (2011).
- [20] X.-L. Qi, Phys. Rev. Lett. **107**, 126803 (2011).
- [21] X. Hu, M. Kargarian, and G. A. Fiete, ArXiv e-prints (2011), arXiv:1105.4381 [cond-mat.str-el].
- [22] J. W. Venderbos, M. Daghofer, and J. van den Brink, Phys. Rev. Lett. **107**, 116401 (2011), 1106.4439.
- [23] Y.-F. Wang, Z.-C. Gu, C.-D. Gong, and D. N. Sheng, ArXiv e-prints (2011), arXiv:1103.1686 [cond-mat.str-el].
- [24] S. Raghu, X.-L. Qi, C. Honerkamp, and S.-C. Zhang, Phys. Rev. Lett. **100**, 156401 (2008).
- [25] G. A. Fiete, V. Chua, X. Hu, M. Kargarian, R. Lundgren, A. Ruegg, J. Wen, and V. Zyuzin, ArXiv e-prints (2011), arXiv:1106.0013 [cond-mat.str-el].
- [26] S. Nishimoto, M. Nakamura, A. O'Brien, and P. Fulde, Phys. Rev. Lett. **104**, 196401 (2010).
- [27] P. Matl, N. Ong, Y. Yan, Y. Li, D. Studebaker, T. Baum, and G. Doubinina, Phys. Rev. B **57**, 10248 (1998).
- [28] Y. Taguchi, Y. Oohara, H. Yoshizawa, N. Nagaosa, and Y. Tokura, Science **291**, 2573 (2001).
- [29] W. Koshibae and S. Maekawa, Phys. Rev. Lett. **91**, 257003 (2003).
- [30] H. F. Pen, J. van den Brink, D. I. Khomskii, and G. A. Sawatzky, Phys. Rev. Lett. **78**, 1323 (1997).
- [31] See Supplemental Material, included here as an appendix.
- [32] B. Normand and A. M. Oleś, Phys. Rev. B **78**, 094427 (2008).
- [33] T. Nomura and K. Yamada, J. Phys. Soc. Jpn. **69**, 1856 (2000).
- [34] I. Martin and C. D. Batista, Phys. Rev. Lett. **101**, 156402 (2008).
- [35] E. Dagotto, *Nanoscale Phase Separation and Colossal Magnetoresistance* (Berlin: Springer, 2002).
- [36] Y. Akagi and Y. Motome, J. Phys. Soc. Jpn. **79**, 083711 (2010).
- [37] D. N. Sheng, Z.-C. Gu, K. Sun, and L. Sheng, Nature Comm. **2**, 389 (2011).
- [38] Y. Kato, I. Martin, and C. D. Batista, Phys. Rev. Lett. **105**, 266405 (2010).
- [39] S. Kumar and J. van den Brink, Phys. Rev. Lett. **105**, 216405 (2010).
- [40] G.-W. Chern, Phys. Rev. Lett. **105**, 226403 (2010).
- [41] R. Shindou and N. Nagaosa, Phys. Rev. Lett. **87**, 116801 (2001).
- [42] N. Regnault and B. A. Bernevig, ArXiv e-prints (2011), arXiv:1105.4867.
- [43] Q. Niu, D. Thouless, and Y.-S. Wu, Phys. Rev. B **31**, 3372 (1985).
- [44] D. Xiao, M.-C. Chang, and Q. Niu, Rev. Mod. Phys. **82**, 1959 (2010).
- [45] H. Takatsu, S. Yonezawa, S. Fujimoto, and Y. Maeno, Phys. Rev. Lett. **105**, 137201 (2010).